

# Modeling and Reduction of Radiated EMI in a GaN IC-based Active Clamp Flyback Adapter

Juntao Yao, *Student Member, IEEE*, Yiming Li, *Student Member, IEEE*, Shuo Wang, *Fellow, IEEE*,  
Xiucheng Huang, *Member, IEEE*, Xiaofeng Lyu, *Member, IEEE*

**Abstract**— This paper first develops a radiated EMI model for a GaN IC-based active clamp flyback converter. Important capacitive couplings, which play a big role in the radiated EMI, are identified, extracted, and validated in the converter. The radiated EMI model is improved to characterize the impact of capacitive couplings. Based on the improved model, techniques to reduce capacitive couplings and the radiated EMI are proposed and experimentally validated.

**Index Terms**—Radiated electromagnetic interference, flyback converter, capacitive coupling, GaN device, active clamp

## I. INTRODUCTION

In modern power electronics, fast-switching Gallium-Nitride (GaN) devices can operate at the switching frequencies higher than conventional Si MOSFETs, so they help significantly reduce the size of passive components and increase power density [1-5]. The active clamp flyback (ACF) converter is a ZVS soft-switching topology, which recycles the energy stored in leakage inductance [6, 7] to improve conversion efficiency. Working with GaN devices, the ACF converter operating at several hundred kHz to 1 MHz could be a game-changer for high power-density and high-efficiency power adapters [8].

However, fast-switching GaN devices lead to high switching noise especially radiated EMI [6, 9-11]. Also, high power-density layout leads to near field couplings which degrade EMI filter performance [12]. Radiated EMI of a power converter has been analyzed in [9, 10, 13, 14]: the long power cables attached to the power converter behave like an antenna [10, 13, 14] driven by the noise generated by the power converter; in isolated power converters, the antenna can be driven by the voltage difference between the primary ground (PGND) and the secondary ground (SGND) [9, 10, 13, 15, 16], which is mainly caused by the unbalanced transformer parasitics. Radiated EMI can be suppressed by reducing the common mode (CM) currents flowing between transformer primary and secondary windings. Techniques such as CM chokes with high-frequency (HF) lossy magnetic cores and coaxial shielding winding transformers can help reduce the radiated EMI [10, 14]; however, due to the parasitics such as parasitic capacitance and inductance, their HF performance has much to desire [12, 17-21]. In a high power-density design, near field couplings can degrade EMI filter performance, so it is important to investigate the couplings within converters [5, 22-24].

This paper investigates the modeling and reduction of radiated EMI. Section II will develop a model for the radiated EMI. In section II A, a preliminary radiated EMI model will be first developed. In section II B, the impact of the capacitive couplings on the radiated EMI will be identified and analyzed. An improved radiated EMI model will be developed to characterize the impact of the capacitive couplings. In section

III, techniques to reduce capacitive couplings and the radiated EMI will be proposed and verified. The investigation in this paper is based on a 60 W GaN IC-based ACF power adapter.

## II. DEVELOPMENT OF THE RADIATED EMI MODEL INCLUDING CAPACITIVE COUPLINGS

Fig. 1 (a) shows a GaN IC-based ACF power adapter above the ground. Fig. 1 (b) shows the prototype photo. The input and output voltages are 120 V AC and 20 V DC respectively. The main and clamping switches, and gate drivers are integrated into Navitas Semiconductor's GaN ICs NV6117 and NV6115. The switching frequency is 450 kHz, and the switching slew rate in this ACF is 20 V/ns. The winding structure of the planar transformer has been optimized to minimize the conductive CM noise [6]. The lengths of the input and output cables are 0.8 m and 0.9 m respectively. The load is a 6.67  $\Omega$  power resistor.

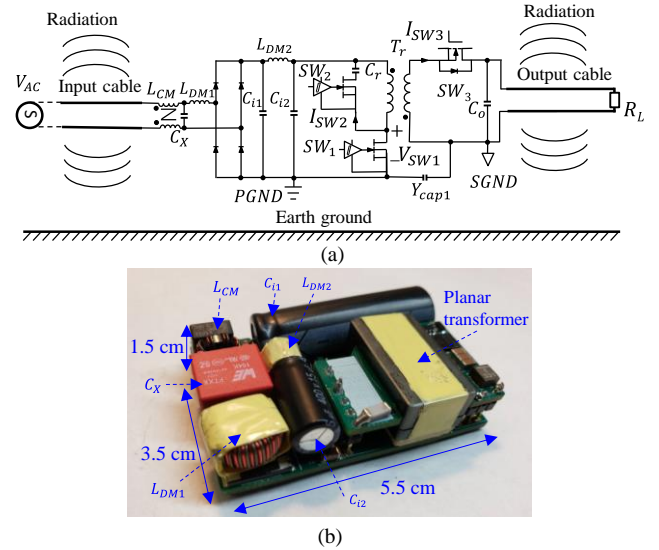


Fig. 1. A GaN IC-based ACF power adapter with power cables attached (a) the circuit (b) the prototype photo.

### A. Preliminary Radiated EMI Model

The radiated EMI is mainly caused by the CM currents flowing on input and output cables. The differential mode (DM) currents of the converter do not significantly contribute to the radiated EMI [9]. Based on the substitution theory,  $SW_1$  can be replaced with a voltage source  $V_{SW1}$ ;  $SW_2$  and  $SW_3$  can be replaced with current sources  $I_{SW2}$  and  $I_{SW3}$  in Fig. 2. Based on the superposition theory, the effect of a voltage/current source on EMI can be analyzed after shorting other voltage sources and disconnecting other current sources. It is found that only  $V_{SW1}$  contributes to the CM noise [24] flowing to the attached input and output cables, causing radiated EMI. As a result,  $I_{SW2}$  and  $I_{SW3}$  can be removed in the model as shown in Fig. 3.

This research was supported by Navitas Semiconductor Inc.

## IEEE TRANSACTIONS ON POWER ELECTRONICS

In Fig. 3, the impedances of capacitors  $C_X$ ,  $C_{i1}$ ,  $C_{i2}$ , and  $C_o$  are assumed to be zero for CM EMI analysis, so  $V_{SW1}$  is directly added to the primary winding of the transformer. Also, one terminal of the primary winding is equivalently connected to PGND. The two conductors of both input and output cables can be treated as one for CM noise analysis. The attached power cables behave like an antenna which can be characterized with an equivalent antenna impedance  $Z_{Antenna}$  [9, 15, 25] in Fig. 4.  $R_r$  is the equivalent radiation resistance,  $R_L$  is the loss resistance of the power cables,  $X_A$  is the reactance representing the near field energy, so  $Z_{Antenna} = R_r + R_L + jX_A$  [25].

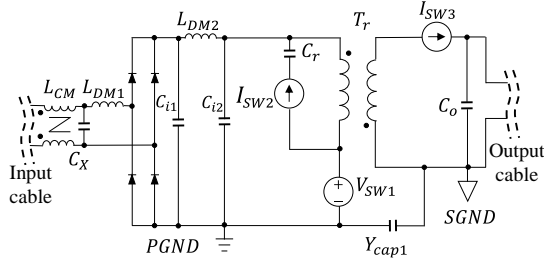


Fig. 2. EMI noise model of an ACF with switching devices substituted by voltage/current sources.

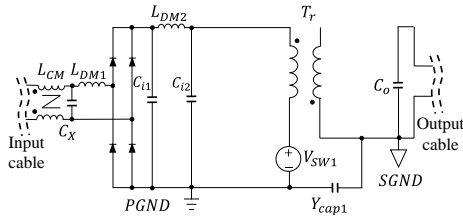


Fig. 3. EMI noise model.

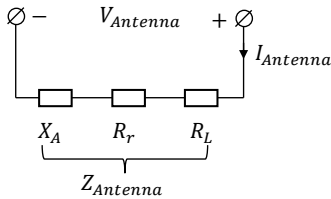


Fig. 4. Equivalent antenna impedance [25].

The measured impedance  $Z_{Antenna}$  of the cable antenna [15] and  $Z_{LCM}$  of the CM choke  $L_{CM}$  are shown in Fig. 5. It should be noted that based on the antenna theory, the antenna impedance includes the effect of the real ground, so the real ground's effect is included in the antenna impedance  $Z_{Antenna}$ .

The CM choke uses a Ni-Zn NL16D core from Hitachi, with an outer diameter 8 mm, an inner diameter 4 mm, a thickness 2 mm, and a 9-turn (AWG26) bifilar winding structure. In the concerned frequency range from 30 MHz to 230 MHz (EN55032 3m class B has the strictest radiated EMI limit in this range),  $Z_{LCM}$ , which is equivalently in series with  $Z_{Antenna}$ , is higher or comparable to  $Z_{Antenna}$  so it can help reduce the CM currents on the antenna.

For the diode-bridge (Z4DGP406L-HF from Comchip Technology) in Fig. 6 (a), when two diodes conduct currents in Fig. 6 (b), the CM impedance of the diode bridge is negligible. In Fig. 6 (c), when all diodes are off, the CM current will flow through diode junction capacitances. Due to the impedance of DM inductor  $L_{DM1}$ , two lines may have different CM currents.

For the worst scenario, when the CM current only flows through the line without  $L_{DM1}$ , the impedance  $Z_{Diode\_bridge}$  of the diode bridge is the two parallel 45-pF diode junction capacitances.  $Z_{Diode\_bridge}$  is much smaller than the impedances of the antenna and  $L_{CM}$ , as shown in Fig. 5. The impedance of the diode bridge can therefore be ignored in the radiated EMI analysis. Also, in Fig. 6 (c), since the diode bridge impedance is ignored, the CM current bypasses  $L_{DM1}$  via the other line, so  $L_{DM1}$  can be ignored.

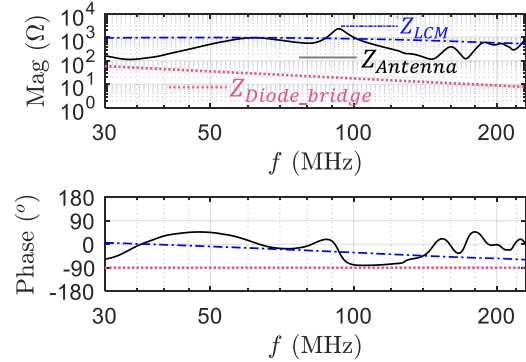


Fig. 5. Extracted impedances of the antenna, CM choke, and diode bridge.

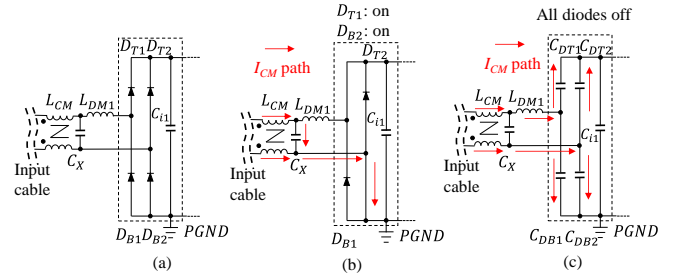


Fig. 6. Impedance of the diode bridge can be ignored for the radiated CM current: (a) the schematic (b) two diodes are on, (c) all diodes are off.

Based on the analysis above, the EMI model with transformer parasitics can be simplified to Fig. 7 (a) with both the impedances of the diode bridge and  $L_{DM1}$  ignored.  $V_{GNDs}$  between PGND and SGND is the excitation voltage to drive  $L_{CM}$  and antenna for EMI radiation. To investigate  $V_{GNDs}$  in Fig. 7 (a),  $L_{CM}$ , input and output cables are removed in Fig. 7 (b). Because any parasitics across PGND and SGND may contribute to  $V_{GNDs}$ , although the impedances of  $C_{i1}$ ,  $C_{i2}$ ,  $C_o$ ,  $C_X$ , the diode bridge and the related PCB trace connections are ignored, they may contribute to the parasitic mutual capacitance across PGND and SGND, so they will be kept on the PCB for the parasitic extraction. Because  $V_{SW1}$  is the equivalent switching voltage source added to the primary winding of the transformer, and the resultant excitation voltage  $V_{GNDs}$  is the voltage difference between PGND and SGND, the circuit including all parasitics between PGND and SGND in Fig. 7 (b) can be modeled as a two-port network: the PGND, which is connected to one of the primary winding's two terminals in Fig. 7 (b), is the reference ground; the other primary winding's terminal, which is connected to  $V_{SW1}$ , is the input port, and the SGND is the output port. The output port voltage is therefore  $V_{GNDs}$ . Based on the network theory, a two-port network can be represented with a  $\pi$  network including  $Z_{TP}$ ,  $Z_{TD}$ , and  $Z_{TC}$  in Fig. 7 (c). Since  $Z_{TP}$  is in parallel with  $V_{SW1}$ , it can be removed. The network is reduced to Fig. 7 (d).  $Z_{TD}$  and  $Z_{TC}$  can be

## IEEE TRANSACTIONS ON POWER ELECTRONICS

extracted via S-parameters [15] using the Copper Mountain planar 808/1 vector network analyzer (VNA) and the results are shown in Fig. 8.

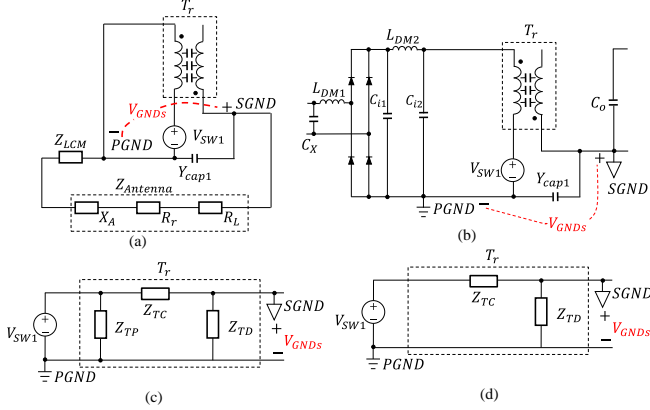


Fig. 7. (a) System EMI model, (b) extraction of parasitics between PGND and SGND with  $L_{CM}$  and cables removed, (c)  $\pi$  model, and (d) reduced model.

In Fig. 8, based on the magnitude and positive phase information,  $Z_{TD}$  behaves like an inductive impedance in the whole frequency range from 30 MHz to 230 MHz.  $Z_{TD}$  is determined by the transformer parasitics, the impedance of  $Y_{cap1}$  and its related parasitic inductance.  $Y_{cap1}$  has an SMD 1808 package with capacitance 1.5 nF. On the other hand, the phase of  $Z_{TC}$  is negative from 30 MHz to 107 MHz, but the polarity changes frequently above 107 MHz.  $Z_{TC}$  is much bigger than  $Z_{TD}$  below 230 MHz, so the transformer's total CM impedance  $Z_{TC}/Z_{TD}$  is mostly determined by  $Z_{TD}$  for this converter.

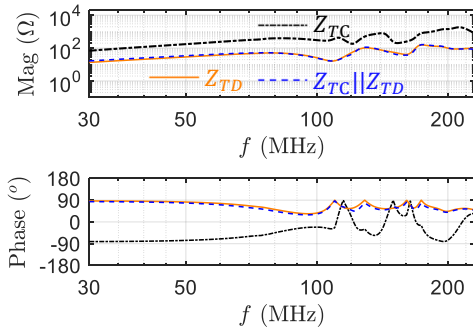


Fig. 8. Extracted impedances.

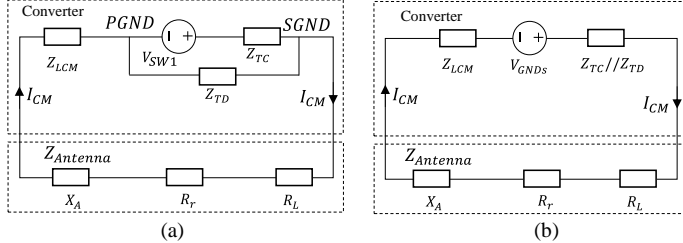


Fig. 9. (a) Preliminary radiated EMI model of the ACF, (b) the reduced model.

With the transformer model in Fig. 7 (d), the radiated EMI model can be developed in Fig. 9 (a), where  $I_{CM}$  is the CM current flowing through the power cables, causing the radiated EMI. Applying Thevenin equivalence between PGND and SGND, it can be further reduced to Fig. 9 (b).  $Z_{TC}/Z_{TD}$  is the Thevenin equivalent impedance. It is much smaller than  $Z_{LCM}$  and  $Z_{Antenna}$  based on Fig. 5 and Fig. 8, so it can be ignored.

## B. Improved Radiated EMI Model Including Capacitive Couplings

In the experiments, it was found that capacitive couplings play a big role in the radiated EMI. The undesired capacitive couplings exist between conductors with pulsating voltage difference, especially between sensitive nodes and noisy nodes. In order to identify possible capacitive couplings in Fig. 1, components and PCB traces with similar voltage levels are identified as voltage nodes in shaded areas in Fig. 10 (a). The explanations of these nodes are in TABLE I. The capacitive couplings between any two nodes are analyzed in Table II.

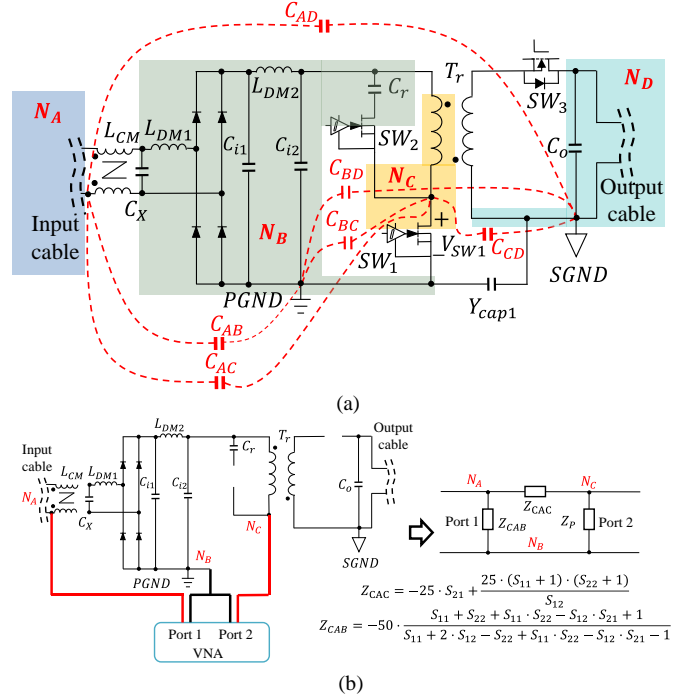


Fig. 10. (a) Identified voltage nodes and capacitive couplings in the ACF, (b) extraction of  $C_{AC}$  and  $C_{AB}$ .

TABLE I. IDENTIFIED VOLTAGE NODES

Node	Components and PCB traces with a similar voltage level
$N_A$	Input cable before CM choke (victim)
$N_B$	$C_X$ , $L_{DM1}$ , diode bridge, $C_{i1}$ , $C_{i2}$ , $L_{DM2}$ , and DC bus
$N_C$	Drain of $SW_1$ , source of $SW_2$ , PCB traces and the transformer winding with a gradient voltage
$N_D$	Output DC bus, $C_0$ , and output cable

TABLE II. CAPACITIVE COUPLINGS BETWEEN CM NODES

	Involved nodes	Analyses about the significance
$C_{AC}$	$N_A$ & $N_C$	Couplings from the pulsating node to the victim node can inject noise to the input cable, so it is a critical coupling.
$C_{AB}$	$N_A$ & $N_B$	$C_{AB}$ is in parallel with the CM choke, so it may degrade CM choke performance.
$C_{AD}$	$N_A$ & $N_D$	$C_{AD}$ is part of the antenna composed of input and output cables; it is determined by the test setup. However, an external capacitance between input and output cables can help reduce the antenna impedance and the radiated EMI.
$C_{BC}$	$N_B$ & $N_C$	$C_{BC}$ is in parallel with $SW_1$ , so it does not influence the gain from $V_{SW1}$ to the CM noise and to the radiated EMI.
$C_{BD}$	$N_B$ & $N_D$	Effect of $C_{BD}$ has been included in the extracted $Z_{TD}$ in Fig. 7; if its impedance is much bigger than those of $Y_{cap1}$ and the transformer, it has negligible influence.

$C_{CD}$	$N_C$ & $N_D$	Effect of $C_{CD}$ has been included in the extracted $Z_{TC}$ in Fig. 7; if its impedance is much larger than that of the transformer, it can be ignored.
----------	---------------	--

The extraction of the impedances  $Z_{CAC}$  and  $Z_{CAB}$  of  $C_{AC}$  and  $C_{AB}$  using a two-port VNA is shown in Fig. 10 (b). Before the measurement, the calibration was made to the exact measurement points, so no additional test wires are needed to do the measurement. The effect of the gradient voltage on the transformer primary winding on capacitive couplings is also included in the measurement because the voltage excitation from port 2 is directly added to the primary winding and this voltage is a gradient voltage on the primary winding. It should be noted that, to extract the coupling parasitics due to  $V_{SW1}$ , based on the superposition theory, other switching devices  $SW_2$  and  $SW_3$  are removed. The extracted S-parameters are converted to a  $\pi$  impedance network [23]. The three impedances of the network correspond to  $Z_{CAC}$ ,  $Z_{CAB}$ , and  $Z_P$ .  $Z_P$ , which is the impedance between  $N_C$  and  $N_B$  in Fig. 10 (b), is not needed in the EMI model. Other parasitic capacitances can be extracted similarly.  $C_{AC}$  and  $C_{AB}$  are extracted as 1.05 pF and 0.63 pF. The EPC of the CM choke is 1.29 pF.  $C_{CD}$  and  $C_{BD}$  are extracted as 1.59 pF and 3.7 pF with port 1 connected between  $N_C$  and  $N_B$ , port 2 connected between  $N_D$  and  $N_B$ , and the transformer removed. Their effects have been included in  $Z_{TC}$  and  $Z_{TD}$  as discussed in TABLE II. Based on the analysis in TABLE II, the capacitive coupling  $C_{AC}$  between the victim node  $N_A$  and the pulsating node  $N_C$  is a very important coupling. It should be pointed out that within the radiated EMI frequency range, the voltage along a cable antenna is not constant, so representing the distributed capacitive coupling between a node and a long cable using a lumped capacitance can give a qualitative analysis but not quantitative analysis. However, the qualitative analysis can still help identify important couplings and develop techniques to reduce the coupling and the radiated EMI.

The radiated EMI model is improved from Fig. 9 (a) to include the impedances of  $C_{AC}$  and  $C_{AB}$  in Fig. 11. The improved model is a Wheatstone bridge with  $V_{SW1}$  as the noise source and the antenna impedance as the load. The output voltage  $V_{AD}$  (voltage between nodes  $N_A$  and  $N_D$ ) of the bridge due to the unbalance is the excitation voltage of the antenna. The voltage gain is,

$$\frac{V_{AD}}{V_{SW1}} \approx \left( \frac{Z_{Antenna}}{Z_{LCM} // Z_{CAB} // Z_{CAC} + Z_{Antenna}} \right) \left( \frac{Z_{LCM} // Z_{CAB}}{Z_{LCM} // Z_{CAB} + Z_{CAC}} - \frac{Z_{TD}}{Z_{TD} + Z_{TC}} \right) \quad (1)$$

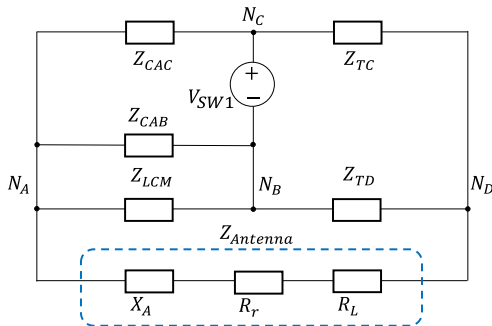


Fig. 11. Radiated EMI model including the capacitive couplings.

In (1), the 2<sup>nd</sup> factor represents the balance condition of the Wheatstone-bridge. Based on the extracted parasitic

impedances in Fig. 5 and Fig. 8, Fig. 12 shows the results of the 2<sup>nd</sup> factor. Compared with the balance curve without  $C_{AC}$ , i.e.  $Z_{TD}/(Z_{TD} + Z_{TC})$  in the same figure, the capacitive coupling  $C_{AC}$  introduces more unbalance, so it greatly increases  $V_{AD}$  and the radiated EMI.

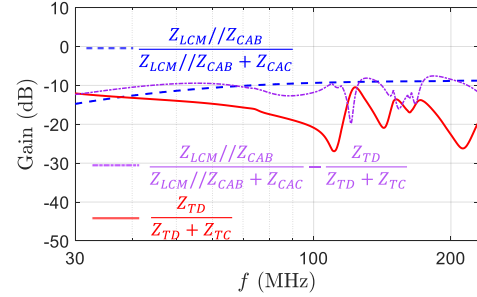


Fig. 12. Capacitive coupling  $C_{AC}$  leads to more unbalance.

### C. Experimental Verification

Based on the preliminary radiation model in Fig. 9 (b), the radiated power  $P_r$  on  $R_r$  can be predicted and the radiated maximum electric field intensity  $E_{max}$  at distance  $r$  from the converter is given by (2) [9] for this preliminary model,

$$E_{max} = \sqrt{\frac{\eta D_o P_r}{2\pi r^2}} = \sqrt{\frac{\eta D_o}{2\pi r^2}} \times \frac{|V_{GNDs}|}{|Z_{Antenna} + Z_{LCM} + Z_{TC} // Z_{TD}|} \sqrt{R_r} \quad (2)$$

where  $\eta$  is the characteristic impedance  $120\pi \Omega$ ;  $D_o$  is the maximum directivity of the antenna at distance  $r$ .

Based on (2), the insertion gain  $IG_{LCM}$  of  $L_{CM}$ , which is defined as the ratio of the radiated  $E_{max}$  with  $L_{CM}$  to that without  $L_{CM}$ , can be derived in (3),

$$IG_{LCM} = \frac{1}{|1 + Z_{LCM} / (Z_{Antenna} + Z_{TC} // Z_{TD})|} \approx \frac{1}{|1 + Z_{LCM} / Z_{Antenna}|} \quad (3)$$

From (3), high  $Z_{LCM}$  can reduce radiated EMI. Fig. 13 shows the calculated insertion gain based on (3).  $L_{CM}$  can reduce radiated EMI by 3 dB to 18 dB from 30 MHz to 230 MHz.

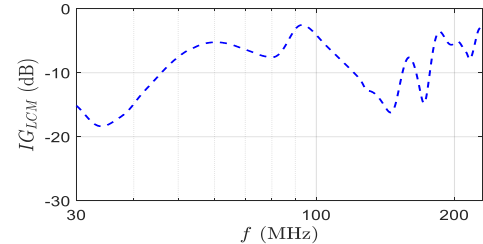


Fig. 13. Calculated insertion gain of the CM choke for the radiated EMI.

The radiated EMI of the ACF is measured in a 3-meter semi-anechoic chamber as shown in Fig. 14, according to the EMI standard EN55032 class B for power adapters. Ferrite beads (Fair-Rite 0431167281) are used on the input cable before the AC plug to isolate the grid from the measurement [15].

Based on the measured EMI without the CM choke and the calculated insertion gain of the CM choke, the radiated EMI with the CM choke is predicted and compared with the measured in Fig. 15. The measured is several dB higher than the predicted above 70 MHz because of the capacitive coupling  $C_{AC}$  as analyzed in Section II B. Furthermore, the radiated EMI cannot meet the EMI limit below 120 MHz.



# IEEE TRANSACTIONS ON POWER ELECTRONICS

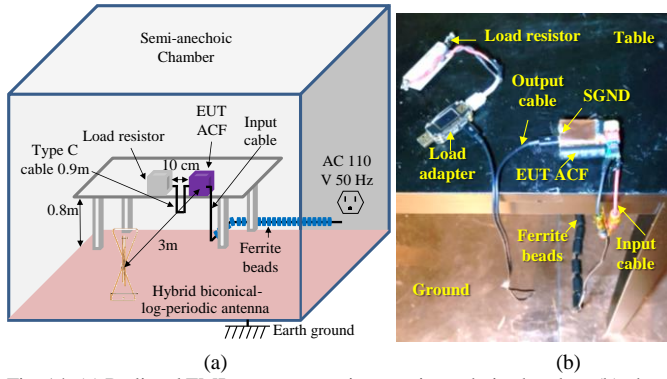


Fig. 14. (a) Radiated EMI measurement in a semi-anechoic chamber, (b) photo.

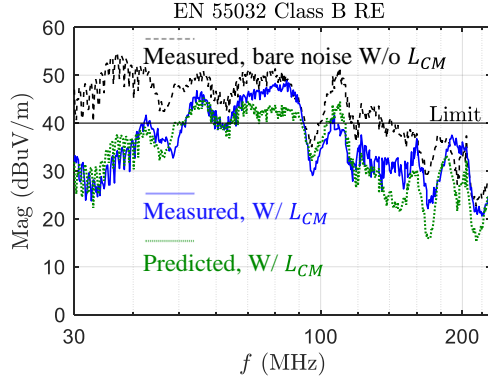


Fig. 15. Comparison of the measured and the predicted radiated EMI.

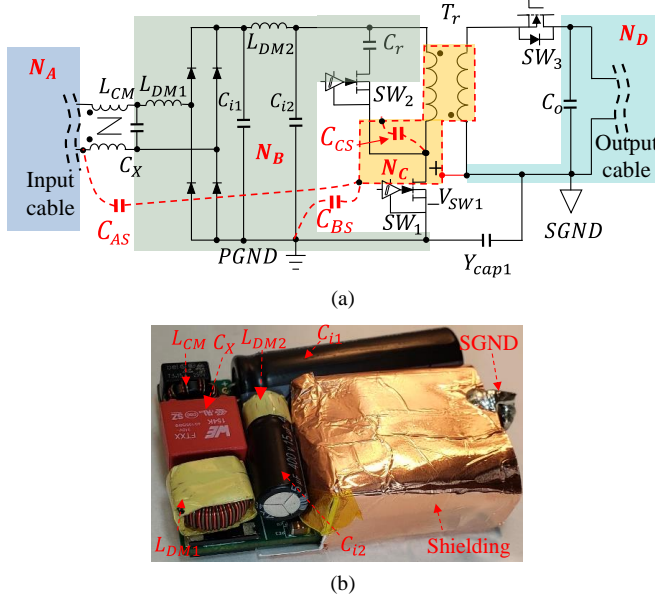


Fig. 16. Applying a shielding to the pulsating node  $N_C$ : (a) circuit and (b) photo.

Based on the analysis in Section II B, the capacitive coupling  $C_{AC}$  should be reduced to reduce the radiated EMI. To validate the impacts of capacitive coupling  $C_{AC}$ , an experiment is conducted in Fig. 16. A copper shielding is applied to node  $N_C$  with the traces and components including the whole transformer identified in TABLE I shielded. The shielding is connected to SGND, so the capacitive coupling between  $N_A$  and  $N_C$  is bypassed to SGND, and the  $C_{AC}$  is eliminated. With the shielding,  $C_{CD}$  and  $C_{BC}$  in Fig. 13 (a) are also eliminated. The parasitic capacitance  $C_{CS}$  and  $C_{AS}$  represent the capacitive

couplings between  $N_C$  and the shielding, and between shielding and  $N_A$ .  $C_{AS}$  is in parallel with  $Z_{Antenna}$ , so it can help reduce the radiated EMI.  $C_{CS}$  is part of  $Z'_{TC}$ .  $C_{BS}$  between the shielding and  $N_B$  is part of  $Z'_{TD}$ . The model is shown in Fig. 17.  $Z'_{TC}$  and  $Z'_{TD}$  can be extracted similar to that of  $Z_{TC}$  and  $Z_{TD}$  in Fig. 7.

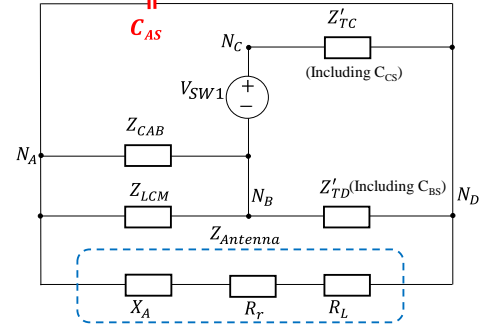


Fig. 17. Radiated EMI model with the node  $N_C$  shielded.

Similar to the extraction of  $C_{BD}$  and  $C_{CD}$  with the transformer removed,  $C_{CS}$  and  $C_{BS}$  are extracted as 1.93 pF and 4.7 pF. They are only slightly bigger than  $C_{CD}$  and  $C_{BD}$ , so  $Z'_{TC}$  and  $Z'_{TD}$  are close to  $Z_{TC}$  and  $Z_{TD}$ . It should be pointed out that because the extracted impedance of  $C_{CS}$  above 160 MHz is determined by high order parasitics, the difference between  $Z'_{TC}$  and  $Z_{TC}$  is bigger above 160 MHz in Fig. 18. The capacitive coupling between the shielding and  $N_D$  is shorted so it does not contribute to the radiated EMI. It should be pointed out that, the shielding should be connected to SGND rather than PGND. If the shielding is connected to PGND, the capacitive couplings between  $N_A$  and the shielding can increase  $C_{AB}$  which degrades the performance of the CM choke.

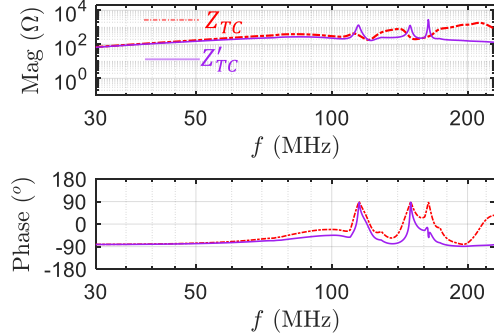


Fig. 18. Comparison of the extracted  $Z_{TC}$  and  $Z'_{TC}$ .

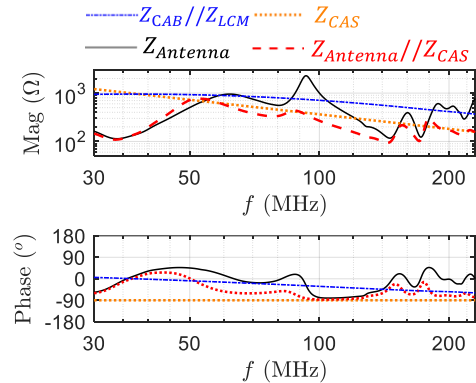


Fig. 19. Impedance comparison.

$C_{AS}$  is extracted as 4.38 pF. It is in parallel with the cable antenna, so the parallel impedance is smaller than the antenna

impedance above 55 MHz as in Fig. 19. Because the parallel impedance is smaller than  $Z_{CAB}/Z_{LCM}$ , based on the model in Fig. 17,  $C_{AS}$  helps reduce the radiated EMI above 55 MHz.

The voltage gain from  $V_{SW1}$  to  $V_{AD}$  is,

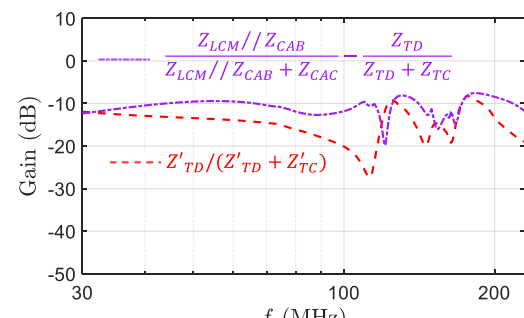
$$\frac{V_{AD}}{V_{SW1}} \approx \left( \frac{Z_{Antenna} // Z_{CAS}}{Z_{CAB} // Z_{LCM} + Z_{Antenna} // Z_{CAS}} \right) \left( \frac{Z'_{TD}}{Z'_{TC} + Z'_{TD}} \right) \quad (4)$$


Fig. 20. Comparison of the 2<sup>nd</sup> factors in (1) and (4).

Comparing (4) with (1), the 1<sup>st</sup> factor in (4) is greatly smaller than that in (1) due to the impedance of  $C_{AS}$ , which will be shown later in Fig. 25 (a). The 2<sup>nd</sup> factor in (4) is also smaller than that in (1) as shown in Fig. 20. The measured radiated EMI in Fig. 21 verified this. In Fig. 21, the radiated EMI with the shielding applied is even lower than the predicted one with  $L_{CM}$  but no capacitive couplings because the shielding not only eliminates the undesired capacitive couplings such as  $C_{AC}$  but also introduces desired capacitive coupling such as  $C_{AS}$ , which helps further reduce the radiated EMI.

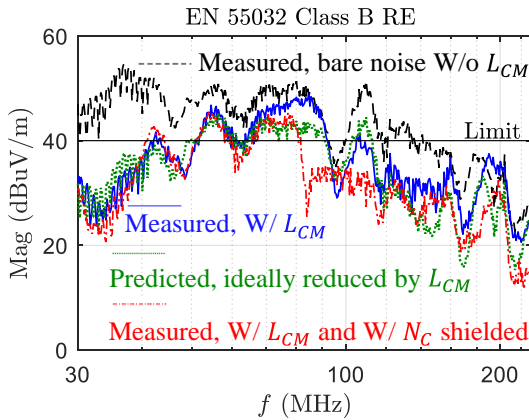


Fig. 21. Measured radiated EMI reduction by shielding  $N_C$ .

However, as shown in Fig. 21, the radiated EMI cannot meet the EMI limit below 80 MHz. It is therefore necessary to develop noise reduction techniques to further reduce the radiated EMI.

It should be noted that the total capacitance  $C_{AS}+C_{BS}+C_{CS}$  between the shielding, which is grounded to the secondary side, and the converter's primary side is around 11pF whose impedance is much higher than the transformer's interwinding impedance and the 1.5 nF Y-capacitor. The effect of  $C_{AS}+C_{BS}+C_{CS}$  on the 50/60 Hz safety leakage current is therefore ignored.

### III. TECHNIQUES TO REDUCE CAPACITIVE COUPLINGS AND RADIATED EMI

#### A. Whole Converter Shielding Technique

Shielding the whole converter with the shielding connected to SGND, as shown in Fig. 22, will have better performance than shielding  $N_C$  because of four reasons: 1)  $C_{AC}$  is eliminated because the whole converter shielding can bypass the capacitive couplings between  $N_A$  and  $N_C$  to SGND; 2)  $C_{AB}$  is eliminated by the shielding because the shielding bypasses the coupling to SGND so  $Z_{LCM}$  is not compromised; 3)  $C_{AS}$  ( $C''_{AS}$  for this case), which is in parallel with the antenna, is increased; 4) the capacitive coupling  $C_{BS}$  between the shielding (SGND) and node  $N_B$  (PGND) is increased to help further reduce the high frequency radiated EMI. For 3) and 4) above, compared with the partial shielding in Fig. 16, the whole converter shielding has a bigger shielding area, is closer to input cable  $N_A$ , and covers much more area of  $N_B$ , including  $C_{i1}$ ,  $C_{i2}$ ,  $L_{DM1}$ ,  $L_{DM2}$ , and the diode bridge, than the partial shielding, so it has a bigger  $C_{BS}$  and  $C_{AS}'' > C_{AS}$ . The parasitics are extracted as  $C_{CS} = 1.93$  pF,  $C''_{AS} = 8.58$  pF, and  $C_{BS} = 11.3$  pF. The radiated EMI model is in Fig. 23. Compared with Fig. 17,  $Z''_{TD}$  is smaller than  $Z'_{TD}$ ;  $Z_{LCM}$  is bigger than  $Z_{LCM}/Z_{CAB}$  and  $C''_{AS}$  is bigger than  $C_{AS}$ . All of these help greatly reduce radiated EMI. In Fig. 24, the impedance of the CM choke is much bigger than the parallel impedance of antenna and  $C''_{AS}$  in the whole frequency range. The voltage gain is,

$$\frac{V_{AD}}{V_{SW1}} \approx \left( \frac{Z_{Antenna} // Z''_{CAS}}{Z_{LCM} + Z_{Antenna} // Z''_{CAS}} \right) \left( \frac{Z''_{TD}}{Z''_{TC} + Z''_{TD}} \right) \quad (5)$$

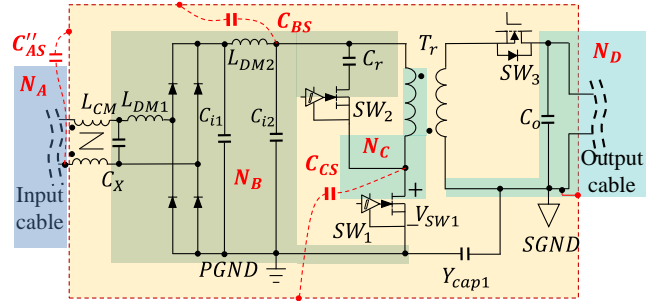


Fig. 22. Applying a shielding to the whole converter.

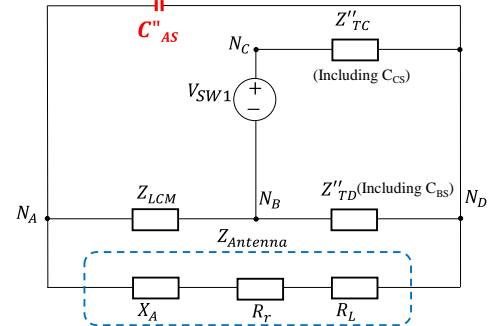


Fig. 23. Radiated EMI model with the whole converter shielded.

Because of  $C''_{AS}$ , the 1<sup>st</sup> factor in (5) is greatly reduced especially above 50 MHz, as shown in Fig. 25 (a). The 2<sup>nd</sup> factor is also reduced. Based on (1), (4), and (5), the predicted voltage gains without shielding, with  $N_C$  shielded, and with the whole converter shielded are compared in Fig. 25 (b). The whole converter shielding gives the lowest voltage gain as predicted by (5).

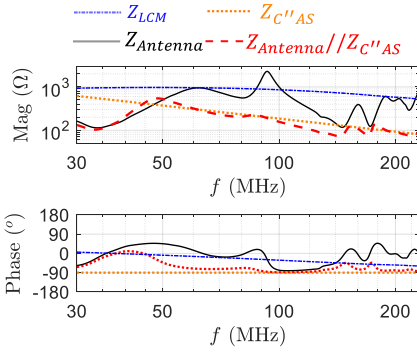


Fig. 24. Impedance comparison.

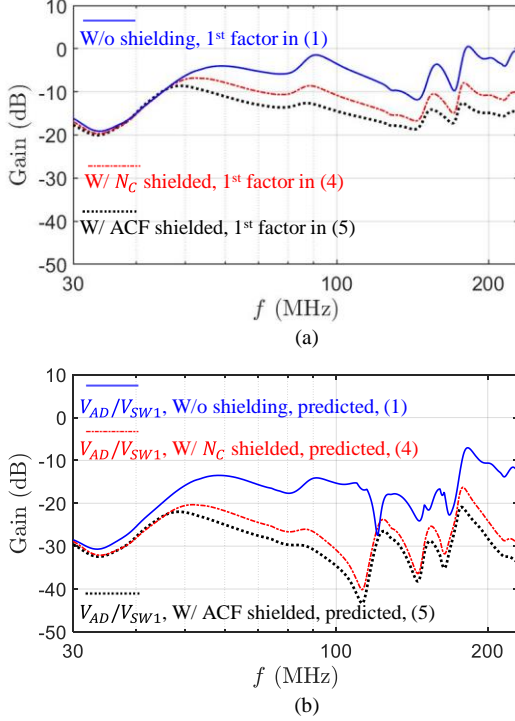


Fig. 25. Comparison of the predicted voltage gains from (1), (4), and (5): (a) comparison of the 1<sup>st</sup> factors (b) comparison of the predicted voltage gains.

The measured EMI is shown in Fig. 26. It is shown that, with the whole converter shielding, the radiated EMI can be further reduced above 50 MHz compared with the  $N_C$  shielding. This validates the analysis. It should be noted that based on the measurements, the shielding does not sacrifice the converter efficiency (93%) because the eddy current due to the leakage magnetic field of the transformer is very small. Similar to the shielding in Fig. 16, the total capacitance  $C_{AS}'' + C_{BS} + C_{CS}$  between the shielding, which is grounded to SGND, and the converter's primary side is around 21.8 pF whose impedance is much higher than the transformer's interwinding impedance and the 1.5 nF Y-capacitor. Its effect on the 50/60 Hz safety leakage current is therefore ignorable.

The predicted radiated EMI reduction in Fig. 25 is larger than the measured in Fig. 26 because, as pointed out in Section II B, the model in Fig. 23 is based on the lumped instead of distributed capacitive couplings, so it gives a qualitative view but not a quantitative view.

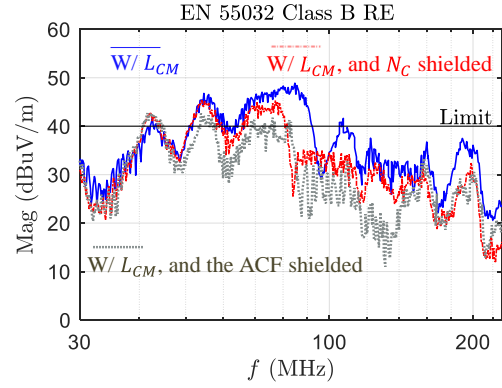


Fig. 26. Radiated EMI reduction by shielding the whole converter.

### B. Improved Whole Converter Shielding Technique

Since the whole converter shielding and the increased  $C_{AS}$  can help reduce the radiated EMI, it is appropriate to add a small capacitor  $Y_{cap2}$  from  $N_A$  to the shielding as shown in Fig. 27 (a) and (b) to increase  $C_{AS}$  on purpose.  $Y_{cap2}$ ,  $L_{CM}$ , and  $Y_{cap1}$  form a CLC CM EMI filter.  $Y_{cap2}$  is connected to SGND via the shielding which has a very small inductance, so it has good HF performance.

The impedance of  $Y_{cap2}$  should be as small as possible to reduce the excitation voltage on the antenna. At the same time,  $Y_{cap1}$  has been designed to meet the conductive EMI standard, so it should be not changed. Because both  $Y_{cap1}$  and  $Y_{cap2}$  generate leakage current from the AC line to DC output,  $Y_{cap2}$  should be kept small to meet safety requirements. In high-frequency range, the equivalent series inductance (ESL) of a Y-capacitor is significantly influenced by the packaging technique. Therefore, a small form factor SMD 1808, 100 pF safety capacitor is selected. The impedance  $Z_{Y_{cap2}}$  including both the impedances of  $Y_{cap2}$  and the shielding from  $N_A$  to  $N_D$  is much smaller than other impedances above 50 MHz in Fig. 28. Because of this, the excitation voltage of the antenna, thus the radiated EMI can be greatly reduced.

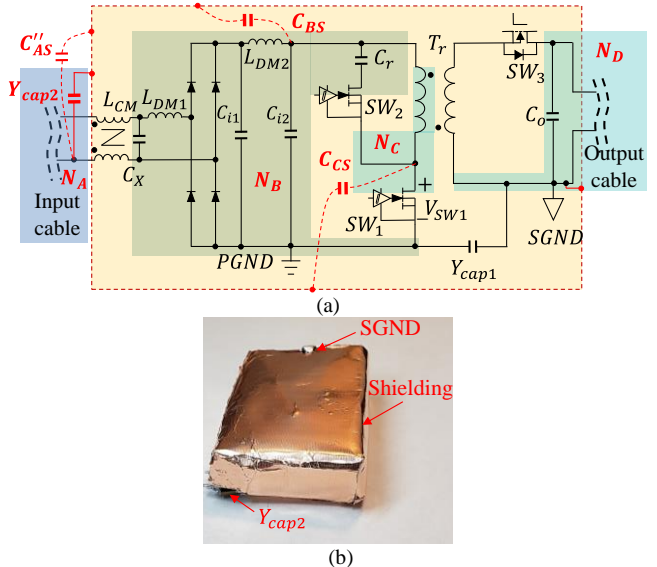


Fig. 27. The proposed CLC shielding CM filter technique: (a) circuit and (b) photo.



## IEEE TRANSACTIONS ON POWER ELECTRONICS

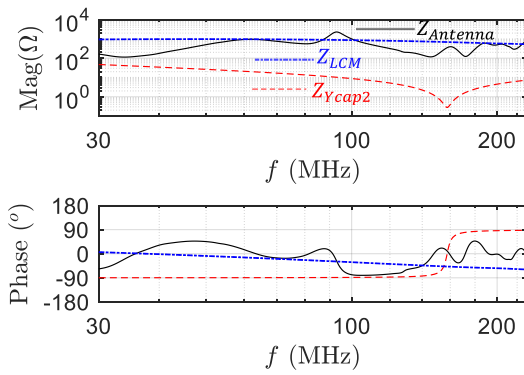


Fig. 28. Impedance comparison.

The measured radiated EMI compared with the other three cases is shown in Fig. 29. In Fig. 29, the radiated EMI is greatly reduced from 40 MHz to 120 MHz compared with that without  $Y_{cap2}$ . It can meet the radiated EMI limit.

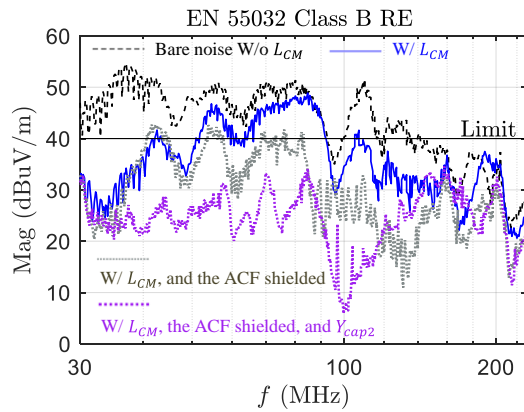


Fig. 29. Radiated EMI with the whole converter shielding and  $Y_{cap2}$ .

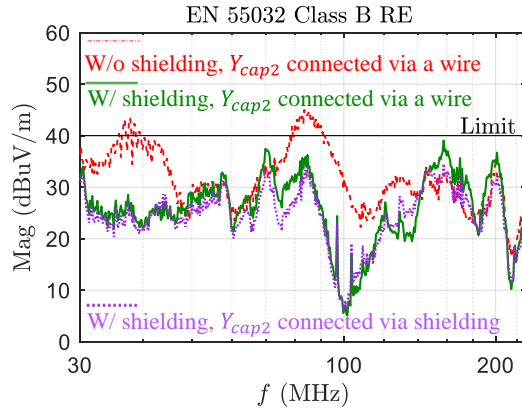


Fig. 30. Radiated EMI comparison of different  $Y_{cap2}$  connection patterns.

When implementing the proposed techniques, a full converter shielding grounded to SGND with  $Y_{cap2}$  connected to the shielding gives the best radiated EMI reduction. Fig. 30 shows the comparison of the measured radiated EMI with different  $Y_{cap2}$  connection patterns. In the first case, without the shielding applied,  $Y_{cap2}$  is directly connected to SGND via a piece of wire. Due to the capacitive couplings  $C_{AB}$  and  $C_{AC}$  as analyzed in section II, the CLC filter ( $Y_{cap2}$ - $L_{CM}$ - $Y_{cap1}$ )'s performance is degraded, so it cannot meet the radiated EMI limit. In the second case, the shielding is applied, but  $Y_{cap2}$  is directly connected to SGND via a piece of wire instead of via the shielding. The radiated EMI is much lower than the 1<sup>st</sup> case.

In the 3<sup>rd</sup> case, the  $Y_{cap2}$  is connected to SGND via the shielding. It leads to the lowest radiated EMI to meet the EMI limit with enough margin.

The proposed techniques are insensitive to different prototypes because of the following: 1) the proposed techniques can eliminate the most important capacitive couplings between  $N_A$  and  $N_C$ , and 2) the parasitic capacitance  $C_{AS}$  between the shielding and  $N_A$  can reduce the radiation because it is in parallel with the cable antenna. Fig. 31 (a) shows the proposed techniques applied to another ACF prototype which has different structures and dimensions from the one in Fig. 1 (b). The measured radiated EMI in Fig. 32 shows that the proposed techniques are very effective.

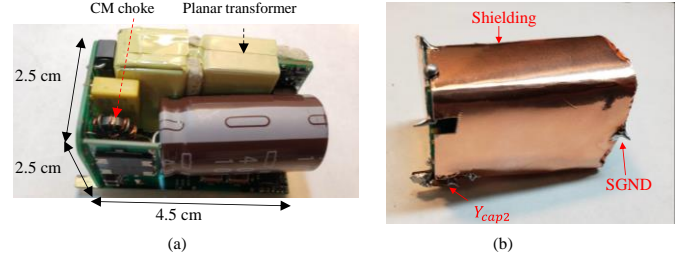


Fig. 31. A different ACF prototype: (a) the photo (b) with a shielding and  $Y_{cap2}$ .

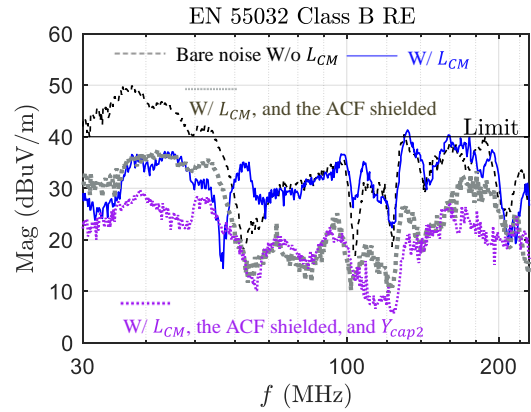


Fig. 32. The proposed techniques reduce radiated EMI regardless of different prototypes.

## IV. CONCLUSIONS

This paper first developed a radiated EMI model for an active clamp flyback converter employing GaN switching devices. It was found that, for the radiated EMI analysis, the switching transformer and the parasitic impedances between the primary and secondary sides can be modeled with two impedances; the impedance of a diode bridge can be ignored no matter it is in on or off status; the capacitive couplings between pulsating voltage nodes and the input and output cables are critical to radiated EMI. Based on the developed model, an improved whole converter shielding technique was proposed to greatly reduce the capacitive couplings and the radiated EMI. Both theoretical analyses and experiments were conducted to validate the proposed modeling and EMI reduction techniques.

## REFERENCES

- [1] X. Huang, Z. Liu, Q. Li, and F. C. Lee, "Evaluation and Application of 600 V GaN HEMT in Cascode Structure," IEEE Trans. Power Electron., vol. 29, no. 5, pp. 2453–2461, May 2014.



# IEEE TRANSACTIONS ON POWER ELECTRONICS

- [2] X. Lyu, Y. Li, D. Cao, S. Jiang, and C. Nan, "Comparison of GaN based switched-tank converter and cascaded voltage divider," in Proc. IEEE 5th Workshop Wide Bandgap Power Devices Appl. (WiPDA), Albuquerque, NM, USA, Oct./Nov. 2017, pp. 158–164.
- [3] B. Li, Q. Li, F. C. Lee, Z. Liu, and Y. Yang, "A High-Efficiency High-Density Wide-Bandgap Device-Based Bidirectional On-Board Charger," IEEE J. Emerg. Sel. Topics Power Electron., vol. 6, no. 3, pp. 1627–1636, Sep. 2018.
- [4] S. Zhao, A. Dearien, Y. Wu, C. Farnell, A. U. Rashid, F. Luo, et al., "Adaptive Multi-Level Active Gate Drivers for SiC Power Devices," IEEE Trans. Power Electron., vol. 35, no. 2, pp. 1882–1898, Feb. 2020.
- [5] B. Zhang and S. Wang, "A Survey of EMI Research in Power Electronics Systems with Wide Bandgap Semiconductor Devices," IEEE J. Emerg. Sel. Topics Power Electron., vol. 8, no. 1, pp. 626–643, Mar. 2020.
- [6] X. Huang, J. Feng, W. Du, F. C. Lee, and Q. Li, "Design consideration of MHz active clamp flyback converter with GaN devices for low power adapter application," in Proc. IEEE Appl. Power Electron. Conf. Expo. (APEC), Long Beach, CA, USA, Mar. 2016, pp. 2334–2341.
- [7] L. Xue and J. Zhang, "Highly Efficient Secondary-Resonant Active Clamp Flyback Converter," IEEE Trans. Ind. Electron., vol. 65, no. 2, pp. 1235–1243, Feb. 2018.
- [8] F. C. Lee, "Keynote 1: Is GaN a Game Changing Device?" in Proc. 2014 16th Int. Power Electron. Motion Control Conf. Expo., Antalya, Turkey, Sep. 2014, pp. 8–14.
- [9] Y. Zhang, S. Wang, and Y. Chu, "Investigation of Radiated Electromagnetic Interference for an Isolated High-Frequency DC–DC Power Converter With Power Cables," IEEE Trans. Power Electron., vol. 34, no. 10, pp. 9632–9643, Oct. 2019.
- [10] J. Yao, Y. Li, H. Zhao, S. Wang, Q. Wang, Y. Lu, et al., "Modeling and Reduction of Radiated Common Mode Current in Flyback Converters," in Proc. IEEE Energy Convers. Congr. Expo. (ECCE), Portland, OR, USA, Sep. 2018, pp. 6613–6620.
- [11] Y. Zhang, S. Wang, and Y. Chu, "Analysis and Comparison of the Radiated Electromagnetic Interference Generated by Power Converters With Si MOSFETs and GaN HEMTs," IEEE Trans. Power Electron., vol. 35, no. 8, pp. 8050–8062, Aug. 2020.
- [12] S. Wang, F. C. Lee, W. G. Odendaal, and J. D. v. Wyk, "Improvement of EMI filter performance with parasitic coupling cancellation," IEEE Trans. Power Electron., vol. 20, no. 5, pp. 1221–1228, Sep. 2005.
- [13] J. Yao, S. Wang, H. Zhao, Y. Zhang, Y. Lu, et al., "Measurement Techniques of CM Currents, Impedance and Voltages for Radiated EMI in Isolated Power Converters," in Proc. IEEE Symp. Electromagn. Compat., Signal Integrity Power Integrity, Long Beach, CA, USA, Aug. 2018, pp. 438–443.
- [14] J. Yao, Y. Li, H. Zhao, and S. Wang, "Design of CM Inductor Based on Core Loss for Radiated EMI Reduction in Power Converters," in Proc. IEEE Appl. Power Electron. Conf. Expo., Anaheim, CA, USA, Mar. 2019, pp. 2673–2680.
- [15] J. Yao, S. Wang, and H. Zhao, "Measurement Techniques of Common Mode Currents, Voltages, and Impedances in a Flyback Converter for Radiated EMI Diagnosis," IEEE Trans. Electromagn. Compat., vol. 61, no. 6, pp. 1997–2005, Dec. 2019.
- [16] H. Zhao, J. Yao, and S. Wang, "A Universal DM/CM Physical Model for Power Transformer EMI Analysis within both Conducted and Radiated Frequency Ranges," in Proc. IEEE Energy Convers. Congr. Expo., Portland, OR, USA, Sep. 2018, pp. 6592–6599.
- [17] S. Wang, F. C. Lee, and J. D. v. Wyk, "Inductor winding capacitance cancellation using mutual capacitance concept for noise reduction application," IEEE Trans. Electromagn. Compat., vol. 48, no. 2, pp. 311–318, May 2006.
- [18] S. Wang, F. C. Lee, J. D. v. Wyk, and J. D. v. Wyk, "A Study of Integration of Parasitic Cancellation Techniques for EMI Filter Design With Discrete Components," IEEE Trans. Power Electron., vol. 23, no. 6, pp. 3094–3102, Nov. 2008.
- [19] Y. Liu, K. Y. See, J. Lai, K. J. Tseng, Y. Liu, C. F. Tong, et al., "FEM modelling of three-phase common mode choke for performance evaluation," in Proc. Asia Pac. Int. Symp. Electromagn. Compat., Shenzhen, China, 2016, pp. 96–99.
- [20] S. Wang and F. C. Lee, "Analysis and Applications of Parasitic Capacitance Cancellation Techniques for EMI Suppression," IEEE Trans. Ind. Electron., vol. 57, no. 9, pp. 3109–3117, Sep. 2010.
- [21] S. Wang, Y. Y. Maillet, F. Wang, R. Lai, F. Luo, and D. Boroyevich, "Parasitic Effects of Grounding Paths on Common-Mode EMI Filter's Performance in Power Electronics Systems," IEEE Trans. Ind. Electron., vol. 57, no. 9, pp. 3050–3059, Sep. 2010.
- [22] F. Costa, C. Gautier, B. Revol, J. Genoulaz, and B. Démoulin, "Modeling of the near-field electromagnetic radiation of power cables in automobiles or aeronautics," IEEE Trans. Power Electron., vol. 28, no. 10, pp. 4580–4593, Oct. 2013.
- [23] S. Wang, F. C. Lee, and W. G. Odendaal, "Characterization and parasitic extraction of EMI filters using scattering parameters," IEEE Trans. Power Electron., vol. 20, no. 2, pp. 502–510, Mar. 2005.
- [24] Y. Li, S. Wang, H. Sheng, and S. Lakshmikanthan, "Investigate and Reduce Capacitive Couplings in a Flyback Adapter With a DC-Bus Filter to Reduce EMI," IEEE Trans. Power Electron., vol. 35, no. 7, pp. 6963–6973, July 2020.
- [25] C. A. Balanis, Antenna Theory: Analysis and Design, 3rd ed. Hoboken, NJ, USA: Wiley, 2016.



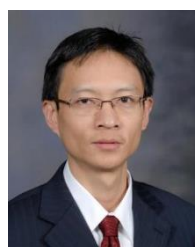
**Juntao Yao** (S'15) received the B.S. and M.S. degrees in electrical engineering from Wuhan University, Wuhan, China, in 2013 and 2016, respectively. He is currently pursuing the Ph.D. degree with the University of Florida, Gainesville, FL, USA.

His research interests include power electronics, electromagnetic interference (EMI), and magnetic components. He has published over 10 IEEE journal and conference papers and holds 1 pending US patent and 9 issued Chinese patents.



**Yiming Li** (S'16) received the B.S.E.E. degree in electrical engineering from Zhejiang University, Zhejiang, China, in 2015, and the Ph.D. degree in electrical engineering from the University of Florida, Gainesville, FL, USA, in 2019. He joined Monolithic Power Systems (MPS) as a Sr. Application Engineer in 2020.

His research interests include electromagnetic interference and compatibility in power electronic systems. He is also studying on transformer and electromagnetic interference filter design and optimization for switching mode power supplies. He has authored and coauthored more than 18 IEEE journal and conference papers since 2017.



**Shuo Wang** (S'03-M'06-SM'07-F'19) received the Ph.D. degree in Electrical Engineering from Virginia Tech, Blacksburg, VA, in 2005. He is currently a full professor with the Department of Electrical and Computer Engineering, University of Florida, Gainesville, FL. Dr. Shuo Wang has published more than 200 IEEE journal and conference papers and holds around 30 pending/issued US/international patents. He received the Best Transaction Paper Award from the IEEE Power Electronics Society in 2006 and two William M. Portnoy Awards for the papers published in the IEEE Industry Applications Society in 2004 and 2012, respectively. In 2012, he received the prestigious National Science Foundation CAREER Award. He is an Associate Editor for the IEEE Transactions on Industry Applications and IEEE Transactions on Electromagnetic Compatibility. He was a technical program Co-Chair for IEEE 2014 International Electric Vehicle Conference.



**Xiucheng Huang** received the B.S. and M.S. degree in electrical engineering from Zhejiang University, China in 2008 and 2011, respectively and the Ph.D. degree from Virginia Tech, Blacksburg, VA, in 2016. He is Sr. Director of Application Engineer of Navitas Semiconductor Inc. since 2016.

His main research interests include Gallium-Nitride semiconductor devices, high-frequency high density power conversion, soft-switching technique, EMI reduction technique, and power architecture. He has issued 3 US patents and 2 Chinese patents, published 2 book chapters, 9 journal papers and 25 conference papers on IEEE Society.

## IEEE TRANSACTIONS ON POWER ELECTRONICS



**Xiaofeng Lyu** received his B.S. degree in 2010 from Nanjing University of Aeronautics and Astronautics (NUAA) and M.S. degree in power electronics from Zhejiang University (ZJU), Hangzhou China, in 2013. He once worked at General Electric (GE) Shanghai, Joulwatt Hangzhou and John Deere Electronic Solutions (JDES), Fargo. He finished his Ph.D. degree in North Dakota State University (NDSU), Fargo, in Dec. 2017. He is now Staff Applications Engineer in Navitas Semi. Inc, Los Angeles.

His research interests include SiC high-density inverters, switched-tank converter for data center, multilevel converter, LED driver and ACF GaN adapter.